

A Journal of the Gesellschaft Deutscher Chemiker

Angewandte Chemie

GDCh

International Edition

www.angewandte.org

Accepted Article

Title: Host-Guest Interactions in Metal-Organic Framework Isorecticular Series for Molecular Photocatalytic CO₂ Reduction

Authors: Philip M. Stanley, Johanna Haimerl, Christopher Thomas, Alexander Urstoeger, Michael Schuster, Natalia B. Shustova, Angela Casini, Bernhard Rieger, Julien Warnan, and Roland A. Fischer

This manuscript has been accepted after peer review and appears as an Accepted Article online prior to editing, proofing, and formal publication of the final Version of Record (VoR). This work is currently citable by using the Digital Object Identifier (DOI) given below. The VoR will be published online in Early View as soon as possible and may be different to this Accepted Article as a result of editing. Readers should obtain the VoR from the journal website shown below when it is published to ensure accuracy of information. The authors are responsible for the content of this Accepted Article.

To be cited as: *Angew. Chem. Int. Ed.* 10.1002/anie.202102729

Link to VoR: <https://doi.org/10.1002/anie.202102729>

COMMUNICATION

Host-Guest Interactions in Metal-Organic Framework Isorecticular Series for Molecular Photocatalytic CO₂ Reduction

Philip M. Stanley,^[a,b] Johanna Haimerl,^[a,c] Christopher Thomas,^[b] Alexander Urstoege,^[d] Michael Schuster,^[d] Natalia B. Shustova,^[c] Angela Casini,^[e] Bernhard Rieger,^[b] Julien Warnan,^{*[a]} and Roland A. Fischer^{*[a]}

- [a] P. M. Stanley, J. Haimerl, Dr. J. Warnan*, Prof. Dr. R. A. Fischer*
Chair of Inorganic and Metal-Organic Chemistry, Department of Chemistry,
Technical University of Munich,
Lichtenbergstraße 4, Garching, Germany
E-mail: julien.warnan@tum.de, roland.fischer@tum.de
- [b] P. M. Stanley, C. Thomas, Prof. Dr. B. Rieger
WACKER-Chair of Macromolecular Chemistry, Department of Chemistry,
Technical University of Munich,
Lichtenbergstraße 4, Garching, Germany
- [c] J. Haimerl, Prof. Dr. N. B. Shustova
Department of Chemistry and Biochemistry,
University of South Carolina,
Columbia, South Carolina, USA
- [d] A. Urstoege, Prof. Dr. M. Schuster
Division of Analytical Chemistry, Department of Chemistry
Technical University of Munich,
Lichtenbergstraße 4, Garching, Germany
- [e] Prof. Dr. A. Casini
Chair of Medicinal and Bioinorganic Chemistry, Department of Chemistry
Technical University of Munich,
Lichtenbergstraße 4, Garching, Germany

Abstract: A strategy to improve homogeneous molecular catalyst stability, efficiency, and selectivity is immobilization on supporting surfaces or within host matrices. Here, we examine the immobilization of CO₂ reduction catalyst [ReBr(CO)₃(4,4'-dcbpy)] and photosensitizer [Ru(bpy)₂(5,5'-dcbpy)]Cl₂ using the isorecticular series of metal-organic frameworks (MOFs) UiO-66, -67, and -68. Specific host pore size choice enables distinct catalyst and photosensitizer spatial location – either at the outer MOF particle surface or inside the MOF cavities – affecting catalyst stability, electronic communication between reaction centre and photosensitizer, and consequently the apparent catalytic rates. These results allow for a rational understanding of optimized supramolecular layout of catalyst, photosensitizer, and host matrix.

Introduction

Catalysis will continue to be central to address global challenges including rising energy consumption, environmental pressures, and industrial chemical synthesis, promoting research toward efficient systems.^[1] In artificial photosynthesis based on molecular catalysts significant progress has been made in the past decades, however, metal complex instability under reaction conditions remains challenging.^[2,3] Immobilizing molecular catalysts from homogeneous solution on support materials and providing synergistic host environments are potential solutions toward improved catalyst performance and recyclability.^[2,4]

Metal-organic frameworks (MOFs) are particularly interesting (model) supports as their modular building principle offers a myriad of topologies, cavity sizes, and molecular catalyst inclusion capabilities.^[5,6,7] Such MOF-based supramolecular host-guest-systems have been extensively studied for catalytic reactions from fine chemical synthesis to photocatalysis.^[8,9] Solar fuel generation strategies involving MOFs include hosting, photoresponsive materials, encapsulation, and scaffolding.^[10,11,12]

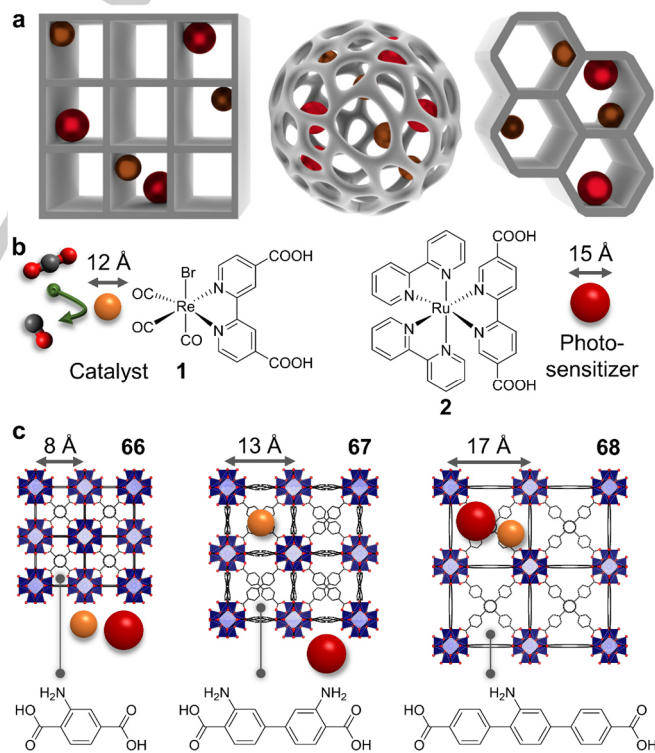


Figure 1. a Representation of integrated molecular photosystems (spheres) in various assembly-controlling MOF topologies. b Structures of CO₂ reduction catalyst [ReBr(CO)₃(4,4'-dcbpy)] (1) and photosensitizer [Ru(bpy)₂(5,5'-dcbpy)]Cl₂ (2). c Anchoring sites of 1 and 2 in the isorecticular UiO (66, 67, 68) host series based on pore sizes and the respective MOF linkers.

COMMUNICATION

Alongside other hosting materials (e.g., micelles, particles, covalent organic frameworks), MOF-based systems can display an abundance of diversity in pore size, surface area and topologies (Figure 1a) that deeply condition the electronic communication efficiency between the (photo)electroactive species.^[13] Although few studies have started careful exploration of MOF parameters on (photo)catalytic performance, e.g., promoting intermediates in engineered MOF pores, the understanding of host-guest effects, specific anchoring sites, and reactive center distances for molecular catalysts in solar fuel production remains limited.^[14,15] Herein, we rationally conceived a host-guest system to correlate reactivity with spatial location in MOF-entrapped molecular photosystems. Two distinct approaches were employed: (i) specific surface modification through grafting and/or entrapping of molecular photosystems, and (ii) variation of average distance between catalysts and photosensitizers via tuning their molecular ratio. This was achieved through designing, synthesizing, and evaluating a supramolecular photosystem/MOF series which systematically differs threefold in microstructure enabled by varying MOF cavity sizes (Figures 1b-c).

The chemically stable UiO MOF family, composed of $Zr_6O_4(OH)_4$ nodes and terephthalic acid derived expanded linkers forming UiO-66, -67, and -68, was chosen as the model matrix.^[16] These MOFs exhibit a wide range of maximum pore diameters of 8.0, 13.1, and 17.2 Å, respectively (Figure 1c), which enables systematic, pore size dependent, photocatalysis investigations.^[17] As molecular photosystem components, the CO_2 reduction catalyst $[ReBr(CO)_3(4,4'-dcbpy)]$ (dcbpy = dicarboxy-2,2'-bipyridine) (**1**) and the photosensitizer $[Ru(bpy)_2(5,5'-dcbpy)]Cl_2$ (bpy = 2,2'-bipyridine) (**2**) provide a well-studied benchmark delivering modest homogeneous catalyst activity with a sacrificial electron donor (SED).^[18–20] Carboxyl groups on the dcbpy ligands were chosen to anchor **1** and **2** at the MOF via its nodes and its amine-modified linkers. The latter has shown stable anchoring yielding colloidal systems where photoinduced electron transfers from light-absorbing units to neighboring catalysts in presence of a SED occur.^[10,12,21] These rational host/guest choices allow us to precisely study CO_2 reduction through **1/2** loading variations on MOF outer particle surfaces' or inside the cavities, in relation to host pore diameter and molecular size of **1** and **2**.

Results and discussion

Molecules **1** and **2** were synthesized from literature and characterized (Supporting Information, SI; Figure S1).^[18,22] **1**'s reduction potential, $E(1/1^-)$, is -0.94 V vs saturated calomel electrode (V_{SCE}).^[20] Light excitation of **2** yields the triplet excited state with $E(^32^*/2^-) = 1.07$ V_{SCE} allowing oxidation of triethanolamine (TEOA) ($E(TEOA^+/TEOA) = 0.59$ V_{SCE}) used as a SED.^[23–25] As $E(2/2^-) \approx -1$ V_{SCE} , exergonic electron transfer to **1** is possible triggering CO_2 reduction.^[24–26] Amine-modified UiO-66-NH₂ (**66**), UiO-67-NH₂ (**67**) and UiO-68-NH₂ (**68**) were synthesized following modified literature procedures (SI).^[15,27] The obtained samples showed powder X-ray diffraction (PXRD) reflexes matching simulated patterns from single crystals, confirming crystallinity (Figure S2). Density-functional theory (DFT) calculations on **1** and **2** yielded van der Waals spheres of 12.0 and 14.5 Å, respectively – larger than the maximum pore diameter of **66**, but smaller than **68**, with **67** in between (Figures 1b-c, S3-4).

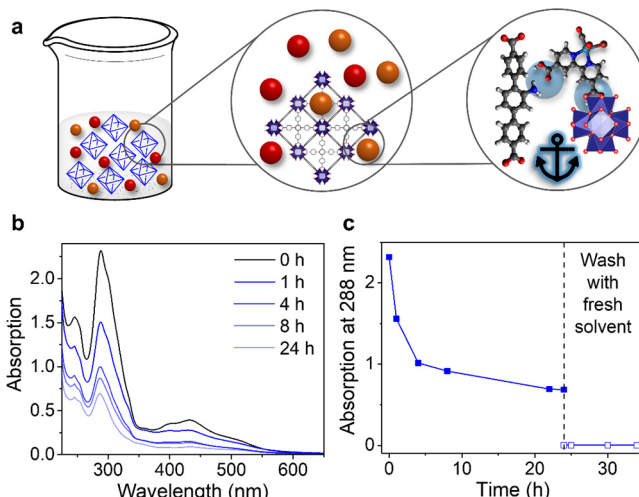


Figure 2. Immobilization of molecular complexes in MOFs. **a** Figurative **68** MOFs (octahedra) with dissolved complexes (spheres). **b** Exemplary ReRu-66 data: Supernatant UV-Vis spectroscopy over time of **66** (10.0 mg) and MeCN (16 mL) with **1** (0.050 mM) and **2** (0.025 mM). **c** Time-absorption at 288 nm during immobilization and during washing.

Non-covalent immobilization of **1** and **2** was achieved by immersing **66**, **67**, or **68** in an acetonitrile (MeCN) solution (details in SI, p. S14) with a defined **2/1** ratio (Figure 2a, Tables S1-3).^[10,12,21] Loading was tracked by supernatant UV-Vis spectroscopy, showing strong absorption decreases in all cases reaching a plateau after 24 h (Figures 2b, S5-6). To verify stable anchoring, the assemblies were then placed in pure MeCN and no supernatant absorption was detected after 10 h, indicating no complex leaching (Figures 2c and S6). Two further control experiment sets, one with CO_2H -free molecular complexes and one with NH_2 -free MOFs, suggested that complex acid groups are essential for amine- and node-anchoring and MOF amines are required for internal cavity hosting (SI p. S14, Figures S7-8).

Table 1. Assembly ICP-MS, loading calculation, and BET data.

	66 -based	67 -based	68 -based
Loading (nmol·mg _{MOF} ⁻¹)			
ReRu-MOF ^[a]	59.5 ± 5.4	73.0 ± 4.3	93.0 ± 3.9
Calculated max. surface loading ^[b]	58.4 ± 0.8	47.1 ± 1.0	63.3 ± 1.3
Total pore loading (%) ^[b]	/ (surface)	11.4 ± 0.2 ^[c]	17.0 ± 0.2 ^[d]
BET area (m ² ·g ⁻¹)			
Pristine MOF	959.7 ± 3.9	1755.7 ± 3.7	2406.7 ± 4.8
Re-MOF	294.4 ± 3.9	1550.8 ± 2.6	1384.5 ± 6.0
ReRu-MOF	337.6 ± 0.6 (R _{MOF} 2.7)	1538.8 ± 4.0 (R _{MOF} 0.4)	287.1 ± 0.8 (R _{MOF} 2.0)

[a] Average max. from ICP-MS, full data in Tables S4-6. [b] See SI. [c] for **Re-67**. [d] for **ReRu-68**(R_{MOF} 2.0).

COMMUNICATION

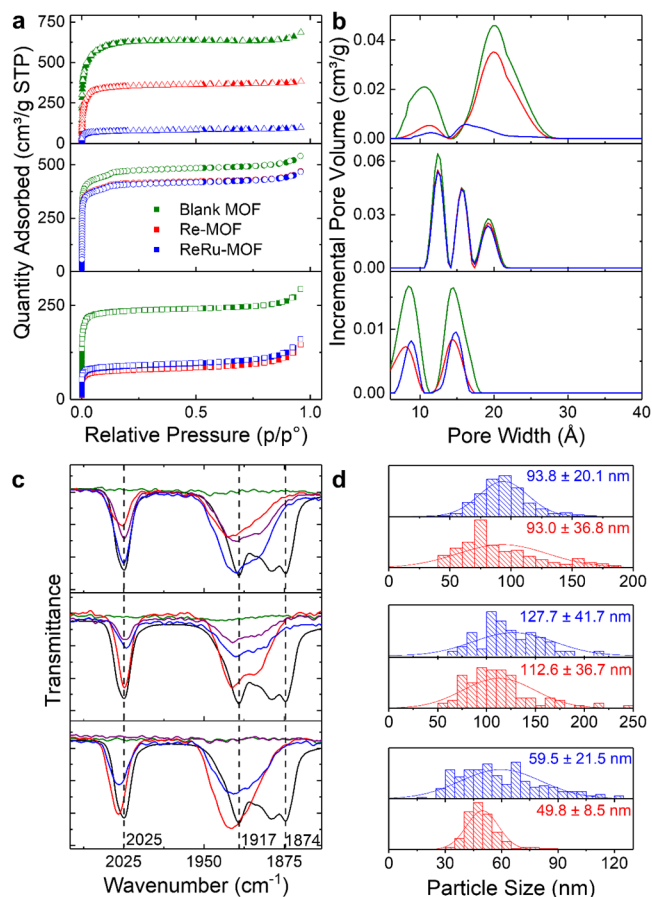


Figure 3. Assembly characterization. **66** (bottom), **67** (middle), **68** (top) with pristine MOFs (green), Re-MOF (red), **ReRu-66**(R_{MOF} 2.7, blue), **ReRu-67**(R_{MOF} 0.4, blue), **ReRu-68**(R_{MOF} 2.0, blue), and corresponding post-catalysis ReRu-MOFs (purple). **a** N_2 adsorption isotherms at 77 K. **b** Calculated pore size distributions. **c** ATR-IR spectra from 1810 to 2075 cm^{-1} of MOF assemblies and pure **1** (black). **d** Particle size histograms from SEM. Bottom to top: **Re-66**, **ReRu-66**(R_{MOF} 2.7), **Re-67**, **ReRu-67**(R_{MOF} 0.4), **Re-68**, **ReRu-68**(R_{MOF} 2.0).

1-loaded, and **1**- and **2**-loaded MOF assemblies, denoted as Re-MOFs and ReRu-MOFs, respectively, were further characterized thoroughly, with the main findings discussed below (more in SI). Precise MOF-entrapped ratio of **2/1** (R_{MOF} , Eq. 1) was determined by inductively-coupled-plasma mass spectrometry (ICP-MS) through Ru and Re quantification yielding average maximum MOF metal loadings increasing from **66** to **67** to **68** (Tables 1, S4-6, Figure S9).

$$\text{Eq. 1} \quad R_{\text{MOF}} = \frac{n(\mathbf{2})}{n(\mathbf{1})} = \frac{n(\text{Ru}_{\text{per mg of MOF}})}{n(\text{Re}_{\text{per mg of MOF}})}$$

PXRD data showed MOF crystallinity retention after molecular immobilization (Figure S2). N_2 gas adsorption experiments displayed significant uptake differences within the series, following isoreticular linker expansion,^[6,7] as well as a decrease in all cases upon immobilizing **1** and **2** (Table 1, Figures 3a and S10). For **66**, pore size distributions (PSDs) revealed that the two pore types decreased by the same volume (Figure 3b). This coverage renders the underlying network harder to access and blocks both pore openings similarly. In contrast, **67**-based PSDs showed an unsymmetrical decrease for different pores upon immobilizing **1** in **Re-67** that remained identical for **ReRu-67**(R_{MOF} 0.4). This is rationalized as the smaller **1** enters the pores, while **2** remains on the outer surface without fully blocking **67**'s pores due to longer

linkers and increased node spacing compared to **66**. Similar PSD decreases for both **Re-67** and **ReRu-67**(R_{MOF} 0.4) are consistent with the internal surface being the main contributor to BET surface area. **68**-based MOFs enable simultaneous **1** and **2** entrapment inside the scaffold in-line with its bigger pore size diameter and apparent from the substantial N_2 uptake decrease and unsymmetrical PSD reduction for **ReRu-68**(R_{MOF} 2.0). We note that **Re-68** displays a surprisingly large BET surface area reduction in comparison to **Re-67**, despite similar loadings, which potentially results from having both tetrahedral and octahedral cavities loaded in **68**.

All materials showed CO_2 uptake that behaves similarly as in N_2 -based experiments (Figure S11). Solid-state UV-Vis spectroscopy of complex-containing MOFs displayed additional bands matching **1** and **2** (Figure S12), supporting retained molecular integrity, albeit with potentially modified photosensitizer absorption properties.^[28] Further, attenuated total reflectance infrared (ATR-IR) spectra for all **1**-loaded MOFs displayed bands at 1917 and 2025 cm^{-1} characteristic of the $\text{Re}(\text{CO})_3$ moiety, highlighting the catalyst's molecular integrity (Figures 3c and S13).^[10,29] Thermal gravimetric analysis revealed earlier degradation on-sets for functionalized MOFs, attributed to the loaded complexes (Figure S14). Scanning electron microscopy (SEM) visualized particles, showing comparable surfaces and sizes pre- and post-immobilization, suggesting no aggregation (Figures 3d, S15-20). This is in-line with calculated crystalline domain sizes and hydrodynamic radii (Figures S21-22).^[30] Calculating MOF surface areas from SEM particle sizes (Figure 3d) with DFT-optimized complexes gave an estimated maximum outer surface loading (Table 1). For **66** this matched experimental values, while actual **67** and **68** provided higher uptake, supporting internal anchoring (Tables S4-6). Further calculations modeled molecular guest interactions with tetrahedral and octahedral pore types and pore loadings (pages S3-4 and Figures S23-27). **1** is hosted by octahedral pores for **67**, by tetra- and octahedral cavities for **68**, while **2** is exclusively loaded into **68**'s octahedral pores. Together with ICP-MS values this suggested that 34% of octahedral pores are occupied in **Re-67**, corresponding to 11% total framework pores (Table 1). For **ReRu-68**(R_{MOF} 2.0) the total loading increases to 17%, with up to 38% of octahedral pores occupied by **2** for photosensitizer-rich **ReRu-68**(R_{MOF} 3.4).

Confocal microscopy images were recorded for **2** and **2**-loaded **66**- and **68**-samples to investigate their spatial luminescence behavior (details in SI, Figures S28-29). While surface-immobilized dye on **66** provided reduced luminescence lifetime estimations compared to pristine **2** with an average photon arrival time (AAT) of 4.13 ± 0.03 and 4.75 ± 0.02 ns, respectively, **68**-entrapped photosensitizer yielded further lifetime reduction with an AAT of 3.67 ± 0.05 ns (Figure S28). Additional experiments on larger **68** crystals (2 μm) enabled spatially resolved luminescence imaging, clearly demonstrating shorter lifetimes from within the crystal than on the surface (Figure S29) and indicating entrapment-induced quenching mechanisms.

Having shown well-defined assembly structures and compositions within the UiO series (Figure 4a), we systematically investigated photocatalytic CO_2 reduction performance and R_{MOF} impact on turnover numbers (TONs), compared to homogeneous conditions. MOF samples in MeCN/TEOA (20/1 v/v) suspension were saturated with CO_2 and irradiated at 450 nm (SI) under vigorous stirring.

COMMUNICATION

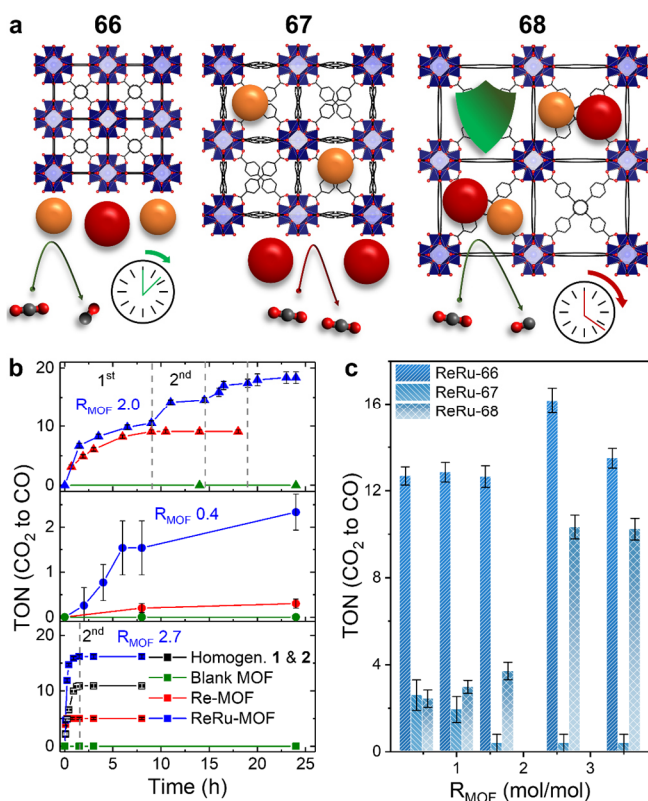


Figure 4. a Schematic concept behind catalytic performance differences. b Accumulated TON vs time plot for **66** (bottom), **67** (middle), **68** (top) with pristine MOFs (green), Re-MOF (red), ReRu-MOF (blue) with best-performing R_{MOF} shown, homogeneous **1** and **2** (black). c First cycle TON vs R_{MOF} .

While particle scattering is expected to impact overall absorption, it is comparable within the series due to similar particle sizes. CO and H₂ formation was monitored via gas chromatography, with no H₂ detected in all runs. CO₂ was the sole source of CO as ¹³C-labelled CO₂ produced only ¹³CO (Figure S30). Control experiments, including pristine MOFs, no SED, or no irradiation yielded no detectable CO (Table S7). All ReRu-66 assemblies showed rapid CO evolution reaching ~16 TONs and deactivating after 1.5 h, due to **1**'s established instability under reaction conditions, further observed from Re(CO)₃ IR band disappearance (Figure 3c).^[31,32] This is superior to homogeneous TONs with **1** and **2**, and **2**-free **Re-66** (TONs ~11 and ~5, respectively) (Figure 4b, Tables S7-8), ascribed to efficient electron transfers between molecular species in direct proximity on **66**'s surface. ReRu-66 samples displayed limited R_{MOF} impact further suggesting electronic communication from **2** to **1** is not performance limiting, but rather **1**'s instability (Figure 4c). In sharp contrast, **Re-67** and ReRu-67 assemblies yielded marginal CO formation over 24 h irradiation with a tenuous R_{MOF} impact. For **Re-67**, and although theoretically possible as TEOA's maximum molecular diameters of 8.6 Å is smaller than **67**'s pore size, this is ascribed to limited TEOA diffusion, reducing efficiency as shown previous reports on immobilized Re catalysts.^[10,12,33,34] Results with ReRu-67 samples are in-line with disabled electron transfer between distant complexes due to the surface-anchoring of **2** and entrapment of **1**. This is supported by decreasing TONs with higher R_{MOF} values, as the probability of having both dye and catalyst surface-anchored decreases with excess **2**. **Re-68** and

ReRu-68 assemblies with $R_{\text{MOF}} > 2.0$ delivered TONs comparable to homogeneous conditions, however over 8 h instead of 1.5 h (Figure 4b). Here R_{MOF} had the strongest impact, as TONs gradually decreased from ~10 to ~2 with lower R_{MOF} . As both complexes load inside the MOF, $R_{\text{MOF}} > 2.0$ ensures sufficient **2** close to **1** on average for efficient CO₂ reduction (Figures 4a,c). Post-catalysis analysis conducted on ReRu-68 samples showed retention of MOF crystallinity and **1**'s integrity (Figures 3c, S2, S21, S22), but substantial Ru leaching (Table S9), suggesting photosensitizer degradation as a main deactivation source.^[10] Consequently, post-catalysis UiO samples were subjected to further immobilization of **2** and more catalysis cycles. Only ReRu-68 samples showed revived activities reaching ~15 TONs after a 2nd cycle. This process was triggered for another two cycles, yielding final accumulated TONs of ~19 after 25 h (Table S10), highlighting **1**'s stabilization inside the scaffold (Figure 4a) and internal anchoring benefits compared to homogenous conditions and surface anchoring, however coupled to a lower apparent turnover frequency. Control experiments where **ReRu-68** ($R_{\text{MOF}} 2.0$) was pre-incubated for 2 h in a CO₂-saturated MeCN/TEOA solution without irradiation yielded comparable CO evolution rates (Figure S31), suggesting that initial SED diffusion is not limiting. Nonetheless, SED replenishment and **2**'s degradation products may contribute to declining rates as slower reaction rates for host-guest photosystems were previously attributed to reaction environment change or transport limitations.^[10,33,35] Additionally, luminescence quenching from pore-entrapment (Figures S28-29) lessens bimolecular electron transfer probabilities potentially resulting in hindered catalysis kinetics.

Finally, replacing TEOA by 1,3-dimethyl-2-phenyl-2,3-dihydro-1*H*-benzo[*d*]imidazole (BIH) as an innocuous SED that maintains pore diffusion (maximum molecular diameter of BIH = 10.6 Å) enabled higher molecular stability and activity.^[12,26] **ReRu-66** ($R_{\text{MOF}} 2.7$) deactivates within 5 h with final TONs of 419 ± 31, clearly outperforming corresponding homogeneous conditions with BIH (TONs = 182 ± 15) (Table S7). ReRu-67 samples showed limited reactivity, while **ReRu-68** ($R_{\text{MOF}} 2.0$) combines reactivity and catalyst stabilization reaching TONs of 506 ± 29 after two 24 h cycles (Table S10). These results further confirm the TEOA-based experiments with the overall prolonged higher activity indicating system limitation by TEOA radicals.^[10,31] This performance compares well to state-of-the-art colloidal MOF systems with TONs in the mid-100s to low 1000s.^[9] In a broader context, our systems are competitive to dye-sensitized TiO₂ semiconductor particles with a surface-anchored ReCl(CO)₃(bpy)-derivative, which reached TONs of 435 in organic solvents with BIH.^[36] Similarly, hosting analogues of **1** and **2** within organosilica nanotubes yielded TONs ~20 with DMF/TEOA under 450 nm irradiation.^[34]

Conclusion

As porous matrices are widely employed to host molecular catalysts, understanding their interactions and correlating reactivity with guest location is key. Thus, we designed the isorecticular MOF series that specifically allows for molecule anchoring to occur on particle surfaces' and/or inside the cavities with different photosystem ratios. Prepared assemblies showed strikingly differing photophysical and photocatalytic behaviors, from partially quenched luminescence upon dye confinement, to rapid CO evolution and catalyst deactivation, over encumbered electronic communication, to lower reaction rates paired with

COMMUNICATION

catalyst shielding and recyclability. These findings show that the guest anchoring site (inside vs outside) and microenvironment design (pore size) has distinct advantages and drawbacks that require a rarely discussed fine tuning. They also shed light on adequacy between the molecular photosystem and MOF host. For the latter, intrinsic structures and guest distances have effects on activity, providing a concept for MOF-based heterogeneous catalyst development. Future studies could investigate covalent guest attachment and consequences on system stability and activity, as well as cage environment fine-tuning to strengthen productive directional charge transfer while suppressing antagonistic quenching channels and mass transport limitations. Our results highlight that host design is paramount, with implications on reactivity, kinetics and stability. Together, these transferrable insights should advance efficient applications at the interface of porous host and molecular catalysis research.

Acknowledgements

P.M.S. thanks the Chemical Industry Fonds for a PhD stipend and Katia Rodewald for SEM. The authors thank Kathrin Kollmannsberger and Lisa Semrau for proof reading. The assistance of Heike Glauner, Alexander Fahrner, and Karl-Heinz Körtje from Leica Microsystems for confocal microscopy is greatly appreciated. There is no conflict of interest to declare. The German Research Foundation (DFG) Priority Program 1928 'Coordination Networks: Building Blocks for Functional Systems' (COORNETs), the research project MOFMOX (FI 502/43-1), and the Excellence Cluster 2089 'e-conversion' supported this work.

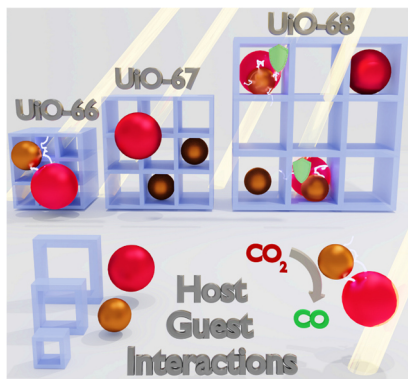
Keywords: Metal-organic frameworks • Solar fuel production • Molecular catalysis • Hybrid materials • Host-guest systems

- [1] Z. Li, S. Ji, Y. Liu, X. Cao, S. Tian, Y. Chen, Z. Niu, Y. Li, *Chem. Rev.* **2020**, *120*, 623.
- [2] X. Liu, S. Inagaki, J. Gong, *Angew. Chem. Int. Ed. Engl.* **2016**, *55*, 14924.
- [3] a) K. E. Dalle, J. Warnan, J. J. Leung, B. Reuillard, I. S. Karmel, E. Reisner, *Chem. Rev.* **2019**, *119*, 2752; b) B. Zhang, L. Sun, *Chem. Soc. Rev.* **2019**, *48*, 2216.
- [4] S. Fukuzumi, Y. - M. Lee, W. Nam, *ChemCatChem* **2018**, *10*, 1686.
- [5] a) S. Kitagawa, R. Kitaura, S.-i. Noro, *Angew. Chem. Int. Ed. Engl.* **2004**, *43*, 2334; b) A. L. Semrau, P. M. Stanley, A. Urstoeger, M. Schuster, M. Cokoja, R. A. Fischer, *ACS Catal.* **2020**, *10*, 3203; c) C. Wang, D. Liu, W. Lin, *J. Am. Chem. Soc.* **2013**, *135*, 13222.
- [6] O. M. Yaghi, M. O'Keeffe, N. W. Ockwig, H. K. Chae, M. Eddaoudi, J. Kim, *Nature* **2003**, *423*, 705.
- [7] H. Furukawa, K. E. Cordova, M. O'Keeffe, O. M. Yaghi, *Science* **2013**, *341*, 1230444.
- [8] H. Konnerth, B. M. Matsagar, S. S. Chen, M. H. G. Precht, F.-K. Shieh, K. C.-W. Wu, *Coord. Chem. Rev.* **2020**, *416*, 213319.
- [9] X. - S. Wang, L. Li, D. Li, J. Ye, *Sol. RRL* **2020**, *4*, 1900547.
- [10] P. M. Stanley, C. Thomas, E. Thyraug, A. Urstoeger, M. Schuster, J. Hauer, B. Rieger, J. Warnan, R. A. Fischer, *ACS Catal.* **2021**, *11*, 871.
- [11] a) A. Dhakshinamoorthy, A. M. Asiri, H. Garcia, *Angew. Chem. Int. Ed. Engl.* **2016**, *55*, 5414; b) M. B. Majewski, A. W. Peters, M. R. Wasielewski, J. T. Hupp, O. K. Farha, *ACS Energy Lett.* **2018**, *3*, 598.
- [12] P. M. Stanley, M. Parkulab, B. Rieger, J. Warnan, R. A. Fischer, *Faraday Discuss.* **2021**, DOI: 10.1039/D1FD00009H.
- [13] C. R. Martin, P. Kittikhunnatham, G. A. Leith, A. A. Berseneva, K. C. Park, A. B. Greytak, N. B. Shustova, *Nano Res.* **2020**, *9*, 19535.
- [14] a) X. Gong, Y. Shu, Z. Jiang, L. Lu, X. Xu, C. Wang, H. Deng, *Angew. Chem. Int. Ed. Engl.* **2020**, *59*, 5326; b) Y. Wang, H. Cui, Z.-W. Wei, H.-P. Wang, L. Zhang, C.-Y. Su, *Chem. Sci.* **2017**, *8*, 775; c) D. J. Xiao, J. Oktawiec, P. J. Milner, J. R. Long, *J. Am. Chem. Soc.* **2016**, *138*, 14371; d) T.-Y. Zhou, B. Auer, S. J. Lee, S. G. Telfer, *J. Am. Chem. Soc.* **2019**, *141*, 1577; e) S. Karmakar, S. Barman, F. A. Rahimi, T. K. Maji, *Energy Environ. Sci.* **2021**, *14*, 2429.

- [15] M. Kaposi, M. Cokoja, C. H. Hutterer, S. A. Hauser, T. Kaposi, F. Klappenberger, A. Pöthig, J. V. Barth, W. A. Herrmann, F. E. Kühn, *Dalton Trans.* **2015**, *44*, 15976.
- [16] J. H. Cavka, S. Jakobsen, U. Olsbye, N. Guillou, C. Lamberti, S. Bordiga, K. P. Lillerud, *J. Am. Chem. Soc.* **2008**, *130*, 13850.
- [17] T. M. Al-Jadir, F. R. Siperstein, *Micropor. Mesopor. Mat.* **2018**, *271*, 160.
- [18] B. W. Pfennig, P. Chen, T. J. Meyer, *Inorg. Chem.* **1996**, *35*, 2898.
- [19] J. Hawecker, J.-M. Lehn, R. Ziessel, *J. Chem. Soc., Chem. Commun.* **1983**, *9*, 536.
- [20] J. M. Smieja, C. P. Kubiak, *Inorg. Chem.* **2010**, *49*, 9283.
- [21] X. Wang, F. M. Wissler, J. Canivet, M. Fontecave, C. Mellot-Draznieks, *ChemSusChem* **2018**, *11*, 3315.
- [22] C.-C. Hou, T.-T. Li, S. Cao, Y. Chen, W.-F. Fu, *J. Mater. Chem. A* **2015**, *3*, 10386.
- [23] H. Sun, M. Z. Hoffman, *J. Phys. Chem.* **1994**, *98*, 11719.
- [24] Y. Pellegrin, F. Odobel, *Cr. Chim.* **2017**, *20*, 283.
- [25] Y. Pellegrin, L. Le Pleux, E. Blart, A. Renaud, B. Chavillon, N. Szuwarski, M. Boujtita, L. Cario, S. Jobic, D. Jacquemin et al., *J. Photochem. Photobiol. A* **2011**, *219*, 235.
- [26] Y. Tamaki, O. Ishitani, *ACS Catal.* **2017**, *7*, 3394.
- [27] a) T. Li, M. T. Kozłowski, E. A. Doud, M. N. Blakely, N. L. Rosi, *J. Am. Chem. Soc.* **2013**, *135*, 11688; b) D. Sun, Y. Fu, W. Liu, L. Ye, D. Wang, L. Yang, X. Fu, Z. Li, *Chem. Eur. J.* **2013**, *19*, 14279.
- [28] M. Sykora, J. R. Kincaid, P. K. Dutta, N. B. Castagnola, *J. Phys. Chem. B* **1999**, *103*, 309.
- [29] A. Vlček in *Topics in Organometallic Chemistry, Vol. 29* (Eds.: A. J. Lees, F. N. Castellano), Springer, **2010**, pp. 115–158.
- [30] A. L. Patterson, *Phys. Rev.* **1939**, *56*, 978.
- [31] S. Meister, R. O. Reithmeier, M. Tschurl, U. Heiz, B. Rieger, *ChemCatChem* **2015**, *7*, 690.
- [32] C. W. Machan, M. D. Sampson, S. A. Chabolla, T. Dang, C. P. Kubiak, *Organometallics* **2014**, *33*, 4550.
- [33] N. M. Orchanian, L. E. Hong, J. A. Skrainka, J. A. Esterhuizen, D. A. Popov, S. C. Marinescu, *ACS Appl. Energy Mater.* **2018**, *2*, 110.
- [34] M. Waki, M. Ikai, Y. Goto, Y. Maegawa, S. Inagaki, *Eur. J. Inorg. Chem.* **2021**, *4*, 1259.
- [35] C. Liu, K. D. Dubois, M. E. Louis, A. S. Vorushilov, G. Li, *ACS Catal.* **2013**, *3*, 655.
- [36] a) E.-G. Ha, J.-A. Chang, S.-M. Byun, C. Pac, D.-M. Jang, J. Park, S. O. Kang, *Chem. Commun.* **2014**, *50*, 4462; b) D.-I. Won, J.-S. Lee, J.-M. Ji, W.-J. Jung, H.-J. Son, C. Pac, S. O. Kang, *J. Am. Chem. Soc.* **2015**, *137*, 13679.

COMMUNICATION

Entry for the Table of Contents



The search for more efficient and stable catalysts often yields hybrid host-guest systems. This work rationally engineered a series of metal-organic frameworks as hosts and selectively positioned guests, a CO₂ reduction catalyst and a photosensitizer, on the surface or inside the pores for photocatalytic solar fuel production. The results obtained help understand host-guest-interactions and provide transferrable criteria for material design.